https://doi.org/10.17113/ftb.63.04.25.8809 original scientific paper

Effect of *Lachnum* YM156 Polyphenol on STAT3/COX-2 Signal Pathway and Gut Microbiota in Mice with N-Nitrosodiethylamine-Induced Hepatic Injury

Running head: *Lachnum* Polyphenol Protects from Hepatic Injury

Tingting Chen[1,§], Dong Liu[1,2,§*] and Ming Ye[1,*]

[1]School of Food and Biological Engineering, Hefei University of Technology, No. 193, Tunxi Road, Hefei City, Postal Code: 230009, China
[2]Anhui Zhanshi Food Corporation, No. 6, South Outer Ring Road, Ningguo City, Postal Code: 242300, China

Received: 3 August 2024
Accepted: 29 September 2025

SUMMARY

Research background. Global food security faces escalating threats from chemical contaminants, with N-nitrosodiethylamine (NDEA) emerging as a potent hepatotoxicant of significant concern. NDEA-induced hepatic injury orchestrates a pathological triad through: (i) reactive oxygen species-

*Corresponding authors:
Phone: +865283135
Fax: +865283135
E-mail: yeming123@sina.com (M.Ye); liudong597855784@aliyun.com (L. Dong)

§Tingting Chen and Dong Liu are co-first authors. Tingting Chen and Dong Liu contributed equally to this work

mediated oxidative cascades, (ii) nuclear factor κB-driven inflammatory amplification, and (iii) Although natural polyphenols demonstrate established protective efficacy, fungal-derived variants remain pharmacologically enigmatic, particularly regarding their pathway-specific regulation and microbiota modulation. We comprehensively investigated the therapeutic capacity of *Lachnum* polyphenols for hepatoprotection.

Experimental approach. The hepatoprotective and microbiota-modulating efficacy of extracellular polyphenol from *Lachnum* YM156 (LSP156) was evaluated in an NDEA-induced mouse model. Sixty male ICR mice were randomised into six experimental groups receiving 28-day oral LSP156 treatment. Body mass measurements, hepatosomatic indices, systemic oxidative stress biomarkers (superoxide dismutase [SOD] and malondialdehyde) and pro-inflammatory cytokines (interleukin [IL]-6 and tumour necrosis factor [TNF]-α) were assessed. Hepatic histopathology was analysed by haemotoxylin and eosin staining, whereas immunoblotting with chemiluminescence detection assessed the STAT3/COX-2 pathway activation. Gut microbiota composition was profiled through 16S rRNA sequencing.

Results and conclusions. After 28-day oral administration (50-100 mg/kg/day), LSP156 significantly improved somatic growth parameters (body mass gain) and organ indices in NDEA-induced mice. LSP156 increased the activities of SOD and catalase, and levels of glutathione, greatly reduced the liver function markers alanine aminotransferase, aspartate aminotransferase, alkaline phosphatase, and total bilirubin, and improved liver cell damage in tissue samples compared to model controls. LSP156 halted the activation of STAT3 and reduced TLR4 levels, which lowered cyclooxygenase protein levels to protect the liver from damage. LSP156 enhanced the digestion and absorption of carbohydrates and proteins, as well as the biosynthesis of terpenoids such as ubiquinone in mice, by rectifying intestinal flora imbalances, modifying the flora structure, and demonstrating a strong correlation between *Bacteroidales* and *Lactobacillales* with the reduction of TNF-α and IL-6. The LSP156 demonstrated dose-dependent therapeutic efficacy in attenuating oxidative stress, hepatocyte impairment, and systemic inflammation.

Novelty and scientific contribution. Fungal polyphenol LSP156 maintains gut bacteria balanced by managing inflammation and oxidation together. These findings outline a new approach for designing drugs targeting multiple factors in complex metabolic disorders.

Keywords: *Lachnum* polyphenol; STAT3/COX-2 signal pathway; gut microbiota; liver injury

INTRODUCTION

N-Nitrosodiethylamine (NDEA), one of the seven N-nitrosamines, is found in food, and it has potential toxicity. Nitrite, which is used as a preservative, produces N-nitrosamines in food (*1-5*). NDEA could induce dozens of diseases in mice, including renal injury (*6*), metabolic disturbances (*7*), liver injury (*8*) and even liver cancer (*9*), and is classified as a 2A carcinogen (probably carcinogenic to humans) by the International Agency for Research on Cancer (*10*). Nitrite, utilised as a preservative, generates N-nitrosamines in food (*1-2*). NDEA can generate numerous disorders in mice, including renal injury (3-4), metabolic abnormalities (*5-7*), liver injury (*8*), and liver cancer (*9*). Cell damage from oxidative stress and free radicals has been recognised as a key reason for the toxicity of NDEA. The free radicals are NDEA metabolites produced by cytochrome P450 families in *vivo*, and their primary metabolic sites are in the liver (*11-12*).

The gut microbiota is influenced by dietary habits, lifestyle, drugs, and other environmental factors and is regulated by genetic genes as well (*13*). The advent of culture-independent sequencing methodologies, including 16S rRNA gene profiling and shotgun metagenomics, has revolutionised high-throughput characterisation of intricate microbial ecosystems (*14*). The gut – liver axis constitutes a pivotal interface in hepatointestinal pathophysiology, with dual mechanistic dimensions. I. Functioning as both a primary immune organ for systemic bacterial clearance and a metabolic nexus for lipid homeostasis, the liver maintains direct anatomical connectivity with the intestinal tract through portal circulation (*15*). Intestinal mucosal immunity regulates innate/adaptive responses, whereas hepatic tissue serves as the initial extraintestinal site processing enteric microbial metabolites and portal venous outflow from both colonic and ileal regions (*16-17*). Gong *et al.* (*16*) reported that gut microbiota influenced the diurnal variation of acetaminophen-induced acute liver injury. Furthermore, the structure of gut microbiota plays a role in systemic inflammation in patients with cirrhosis and NAFLD (*18*).

Polyphenols, natural metabolites extracted from vegetables, fruits, and microorganisms, are obtained through the daily diet, and their powerful antioxidation and free radical elimination properties play an important role in the food industry (*19*). Researchers found polyphenol derived from *Lachnum* sp. had antioxidant and anticoagulant properties (*19-20*). We evaluated the therapeutic effect of LSP156 polyphenols on liver injury and its possible mechanism.

MATERIALS AND METHODS

Materials and reagents

The *Lachnum* YM156 strain, preserved at Hefei University of Technology's Microbial Resource

and Application Research Centre. Mycelium was obtained by fermentation using liquid potato dextrose agar medium, and polyphenol was extracted using a modified protocol (*20*). The fermented mycelium was collected and mechanically homogenised. It was extracted with 70 % ethanol, Tianjing Zhiyuan Chemical Reagent Co., Ltd., Tianjing, China) at a ratio of 1:10 for 4 h. The polyphenol extract was concentrated by rotary distillation at 45 °C for 2 to 3 h. We purified the crude extract using XAD-4 macroporous resin (Rohm & Haas, Philadelphia, USA). The conditions were as follows: the concentration was 10 mg/mL, the flow rate was 2 mL/min, and the eluent was 70 % ethanol. The main fraction was dried in an FD-1B-50 lyophiliser (Beijing Bo Medical Kang Experimental Instrument Co., Ltd., Beijing, China) to obtain LSP156.

ELISA kits (Nanjing Jiancheng Biotechnology Co., Ltd., Nanjing, China) were used to quantify interleukin-6 (IL-6), IL-1 and tumour necrosis factor-α (TNF-α). The test kits for assessing antioxidant glutathione (GSH), catalase (CAT), superoxide dismutase (SOD), malondialdehyde (MDA), and liver injury markers (alanine aminotransferase [ALT], aspartate transaminase [AST], total bilirubin [TBiL], and alkaline phosphatase [AKP]) were provided by Nanjing Jiancheng Biotechnology Co., Ltd. (Nanjing, China).

Animal model preparation

All experimental procedures adhered to the Institutional Animal Care and Use Committee guidelines for animal experimentation. Formal approval was obtained from Hefei University of Technology's Laboratory Animal Welfare and Ethics Committee (approval no. HFTLAWEC20212008). Sixty male ICR mice (SPF grade, 6–8 weeks old) were obtained from Anhui Medical University's Experimental Animal Centre (Hefei, China). The animals were maintained in polypropylene cages under controlled conditions ((24±1) °C, (60±5) % humidity) with ad libitum access to food and water, following a standardised 12-hour light/dark cycle in Hefei University of Technology's animal facility. Following a 7-day acclimatisation period, mice were randomised into six groups (N=8): (1) vehicle control (C), (2) NDEA 100 mg/kg (M), (3) NDEA 100 mg/kg+LSP156 50 mg/kg × 4 weeks (AL), (4) NDEA 100 mg/kg+LSP156 100 mg/kg × 4 weeks (AH), (5) NDEA 100 mg/kg × 4 weeks followed by LSP156 50 mg/kg × 4 weeks (BL), (6) NDEA 100 mg/kg × 4 weeks followed by LSP156 100 mg/kg × 4 weeks (BH). After the treatment period, stool samples were collected, and the mice were sacrificed by neck dissection. Blood was collected from the eyeball and centrifuged to obtain serum, and the tissues of the kidneys, spleen, and liver were dissected and weighed. All materials were stored in a refrigerator at −80 °C.

Measurements of physiological and biochemical indices

The manufacturer's guidelines were employed to measure the oxidative stress parameters, GSH, CAT, SOD, and MDA (Nanjing Jiancheng Biotechnology Co., Ltd., Nanjing, China) in the liver tissue homogenate. The experiments adhered to the guidelines included in the kit. Tissue homogenates were prepared in ice-cold physiological saline (1:9 *m*/*V*) and centrifuged at 3000×*g* for 10 min at 4 °C. The supernatant was collected for assay. Reduced GSH was quantified using the 5,5'-dithiobis-(2-nitrobenzoic acid) reagent: it was incubated at 37 °C for 10 min in darkness, followed by absorbance measurement at 412 nm. GSH content (nmol/mg protein) was derived from a standard curve. The CAT activity was determined by measuring the decomposition rate of H_2O_2 at 240 nm. The activity of SOD was assessed using the WST-8 method at 450 nm and calculated using the inhibition rate. MDA content was measured using thiobarbituric acid at 95 °C for 30 min; absorbance was read at 532 nm and 600 nm after cooling.

The total absorbance was determined using the following formula:

$$A_{total}=A_{532\ nm}-A_{600\ nm} \qquad /1/$$

Liver damage was evaluated by measuring serum activities of AST and ALT, and serum levels of TBil and AKP using commercial assay kits. Liver tissues were homogenised in ice-cold phosphate-buffered saline (1:9 *m*/*V*) and centrifuged (Eppendorf; Vienna, Austria) at 12 000×*g* for 15 min at 4 °C. The supernatant was incubated at 37 °C, and absorbance at 340 nm was recorded at 1 and 2 min using an ultraviolet (UV) spectrophotometer (Shanghai Jinghua Instrument Ltd., China). Enzyme activities were calculated according to the manufacturer's instructions.

The following formula was used for calculating the ALT activity (U per mg protein):

$$\text{ALT activity}=(\Delta A\cdot V_{total}\cdot N)/(\varepsilon\cdot d\cdot V_{sample}\cdot c_{protein}) \qquad /2/$$

where V_{total} refers to the total volume of the reaction solution, N is the dilution factor, ε represents the molar extinction coefficient of NADH ($6.22\cdot10^3$), d denotes the optical path length of the cuvette, V_{sample} is the volume of the sample, and $c_{protein}$ stands for the protein concentration of the liver tissue homogenate.

A volume of 50 µL of a mixed solution containing α-ketoglutarate and aspartate was added to each reaction well, followed by the addition of 10 µL of sample. The mixture was incubated at 37 °C for 30 min. Subsequently, 50 µL of 2,4-dinitrophenylhydrazine chromogenic solution were added and thoroughly mixed, and the reaction was allowed to proceed at 37 °C for an additional 20 min. The reaction was terminated by adding 500 µL of 0.4 mol/L sodium hydroxide solution, with vigorous

mixing. After incubation at room temperature for 10 min, the absorbance (A) of both standard and sample solutions was measured at a wavelength of 510 nm (Shanghai Jinghua Instrument Ltd., China). The measured absorbance values were fitted to a standard curve described by the following polynomial equation:

$$A=0.01907215+303.10147E-2060.8957E^{2.5}+14023.06E^{3} \quad /3/$$

and AST activity (U per g protein) was calculated as:

$$\text{AST activity}=E\cdot 0.482/c_{\text{protein}} \quad /4/$$

where E represents the enzyme activity in Karmen units, 0.482 is the conversion factor from Karmen units to U/L, and c_{protein} denotes the protein concentration in the tissue homogenate expressed in g/L.

TBil (μmol/L) was measured using the diazo method. Aliquots (50 μL) of blank (water), standard (85.5 μmol/L), and sample were mixed sequentially with 1.0 mL of caffeine–sodium benzoate and 0.25 mL of the diazo reagent. After a 10-minute reaction in darkness, the absorbance was read at 530 nm (Shanghai Jinghua Instrument Ltd.).

$$\text{TBil}=(A_{\text{sample}}-A_{\text{blank}})/(A_{\text{standard}}-A_{\text{blank}})\cdot 85.5 \quad /5/$$

The activity of AKP (U/L) was measured using spectrophotometry. Briefly, 20 μL of the sample was mixed with 1.0 mL of the 2-amino-2-methyl-1-propanol buffer (pH=10.4) and 200 μL of p-nitrophenyl phosphate substrate solution for the reaction. The absorbance was measured at 405 nm using a model 752 UV spectrophotometer (Shanghai Jinghua Instrument Ltd.).

$$\text{AKP activity}=(\Delta A/\text{min}\cdot V_{\text{t}}\cdot 1000)/(\varepsilon\cdot V_{\text{S}}\cdot d) \quad /6/$$

The total reaction volume (V_{t}) and sample volume (V_{s}) were 310 and 10 μL, respectively. The pNP molar extinction coefficient (ε) and optical path (d) were $18.5\cdot 10^{3}$ L/(mol·cm) and 1 cm, respectively.

Serum levels of TNF-α, IL-1 and IL-6 were quantified with commercially available enzyme-linked immunosorbent assay kits (Nanjing Jiancheng Biotechnology Co., Ltd.). The serum was isolated by centrifugation (Eppendorf; Vienna, Austria) at 1000×g for 20 min at 4 °C. Subsequently, 100 μL of the standard or serum was incubated at 37 °C for 90 min. After washing, 100 μL of the detection antibody was added and incubated at 37 °C for 60 min. Subsequently, 100 μL of the enzyme conjugate was added and incubated for 30 min at 37 °C. Next, 100 μL of the chromogen was added and developed in darkness for 15 min at 25 °C. The reaction was stopped, and the absorbance was measured at 450 nm (Thermo Electron Corporation; Vantaa™, Finland).

Histopathological assessments

Fresh liver tissues were obtained immediately from different groups of mice, washed with cold normal saline, fixed in 4 % phosphate-buffered paraformaldehyde overnight, dehydrated and embedded in paraffin. Sections (5 μm thick) were selected and stained with haematoxylin and eosin to observe the histopathological changes microscopically (ECLIPSE TE 2000-U; Nikon Instruments Inc., Tokyo, Japan), with images acquired at 400× magnification.

Western blotting analysis

The total protein of the liver sample was extracted using the radioimmunoprecipitation assay buffer and proteinase inhibitor. The protein contents were measured using the bicinchoninic acid protein assay kit (Nanjing Jiancheng Biotechnology Co., Ltd., Nanjing, China). Sodium dodecyl sulfate–polyacrylamide gel electrophoresis was used to separate the protein samples, which were subsequently transferred to a polyvinylidene fluoride membrane (Millipore Inc., Massachusetts, USA) at 300 mA for 0.5 h before being treated with antibodies. The membranes were visualised and scanned using an enhanced chemiluminescence detection system. Photoshop was used to process the images, and Alpha Innotech was used to conduct the assay. ImageJ software version 1.53 (*21*) was used to evaluate protein expression, with relative expression of the protein (REP) determined by normalizing the level of the target protein band (TPB) to that of the actin band (AB).

REP=TPB intensity/AB intensity /6/

16S rRNA gene amplification and MiSeq sequencing

The total genomic DNA was extracted using the DNA Extraction Kit (QIAGEN; cat. no. 12888-100, QIAgen, Hilden, Germany) according to the manufacturer’s instructions, and polymerase chain reaction was performed using barcoded primers and Takara Ex Taq (Takara Bio, Inc., Japan). MiSeq sequencing and bioinformatics analysis of intestinal flora were assisted by Shanghai Meiji Biomedical Technology Co., Ltd. (Shanghai, China). The raw sequencing data were preprocessed using Trimmomatic software (*22*), and QIIME software v. 1.8.0 (*23*) was subsequently employed for further analysis. Primer sequences were removed, and valid tags were clustered into operational taxonomic units (OTUs) with 97 % similarity using Vsearch software (*24*).

Statistical analysis

Data are presented as mean ± standard deviation. The threshold for statistical significance was

established at $p<0.05$. Statistical significance was assessed by one-way analysis of variance (ANOVA) using GraphPad Prism v. 8.0 (*25*).

RESULTS AND DISCUSSION

Effect of LSP156 on injury markers and histopathological examination

Table 1 demonstrates that the activities of ALT, AST and AKP, and concentration of TBiL were significantly elevated in NDEA-induced animals ($p<0.05$) compared to group C, whereas LSP156 therapy dramatically reduced the levels of liver injury indicators ($p<0.05$). Elevated hepatic transaminases (ALT and AST) and cholestatic markers (AKP and TBiL) quantitatively reflected hepatocellular damage progression, corroborating established hepatotoxicity models. NDEA-induced hepatotoxicity correlated with histopathological alterations including lobular inflammation, bridging fibrosis and steato-necrotic changes (*26*). These hepatic enzymes serve as established biomarkers of hepatic dysfunction, with elevated activities directly indicating disrupted membrane integrity and subsequent necrosis through the pathophysiological continuum (*27*). Liu *et al.* (*28*) reported that Tuocha polyphenols could reduce the activities of ALT, AST and AKP and levels of blood lipids. LSP156 also played a positive and effective role in liver injury. Concurrently, morphological alterations in the liver tissue sections of the model group, including nuclear hypertrophy, lipid vacuoles, inflammatory cell infiltration and lobular disarray, were observed, suggesting that NDEA therapy can induce significant hepatic cellular damage. Furthermore, sinus dilatation, eosinophilic bodies, localised necrosis and several nuclear densifications were identified, whereas these injuries were mitigated in LSP156-treated mice (Fig. 1). The hepatotoxicity of NDEA in ICR mice was substantiated by assessing the biomarkers indicating histological abnormalities, hepatocyte necrosis and inflammatory responses, whereas the extent of liver damage was corroborated using organ indices and oxidative damage (*26*,*28*).

Effects of LSP156 on purtenance indexes and oxidative stress markers

NDEA exposure induced hepatotoxicity and carcinogenic potential in mice (*8*). Its systemic effects were assessed by studying the weight gain, organ index and oxidative damage in the model group, which were different from those in the normal group (Table 2). The mean body weight gain of NDEA-treated mice was (5.31±2.44) g, compared to (12.07±1.22) g in control mice. Treatments in the AL, AH, BL, and BH groups can ameliorate the weight gain and organ index in liver injury mice. LSP156 slightly reduced the liver index in both the low- and high-dose groups (AL, AH, BL and BH); however, no significant difference ($p>0.05$) was observed. LSP156 had no meaningful impact on the renal index.

The spleen indices of the AL and AH groups were marginally higher than those of the model group, whereas the BL and BH groups were relatively stable. Another source of NDEA-induced liver damage is a shift in antioxidant enzymes and antioxidant levels. Compared with the control group, the activities of SOD, CAT, and GSH in the NDEA group decreased by 17, 27 and 30 %, respectively, whereas the level of MDA was significantly increased (Table 2). After LSP156 treatments, either as a dietary supplement or as a therapeutic drug, the activities of SOD, CAT, and GSH increased, whereas MDA decreased. The levels of SOD and MDA in the BH group demonstrated marked changes, indicating the best oxidative stress effects among the groups. These results indicated that LSP156 can enhance the antioxidant activity by improving body weight and immune organ index, as well as having a significant regulatory effect on the antioxidant capacity. Therefore, we believe that the anti-inflammatory and antioxidant activity of LSP156 is important in liver-injured mice. NDEA, a hepatocarcinogenic compound, induces oxidative imbalance through reactive oxygen species (ROS) overproduction, triggering hepatic injury and inflammatory cascades (*29,30*). Compromised antioxidant defences enable ROS accumulation beyond cellular neutralisation capacity, initiating DNA damage, membrane disruption, and lipid peroxidation via oxidative stress-mediated pathways (*31-32*).

Effect of LSP156 on regulating the inflammatory signaling pathway

Serum TNF-α, IL-1, and IL-6 were quantified to assess inflammatory involvement in NDEA-induced hepatotoxicity and hepatoprotective efficacy of LSP156. Fig. 2a demonstrates marked elevations of these cytokines in the group M versus controls (C), with significant attenuation following LSP156 treatment, suggesting partial resolution of hepatic inflammation. Mechanistic investigation of LSP156's therapeutic potential against NDEA-mediated liver injury revealed altered phosphorylation status and expression of STAT3/COX-2 axis mediators (cyclooxygenase-2 [COX-2], STAT3 and TLR4) by western blotting. The STAT3 expression was similar in all groups, as shown in Fig. 2b and Fig. 2c, and the expression of p-STAT3, COX-2 and TLR4 in the group M was increased compared with those in the normal group. Correspondingly, p-STAT3/STAT3 revealed a similar variation. However, after LSP156 supplementation, their expression of p-STAT3/STAT3 decreased to varying degrees, particularly in the AH and BH groups (Fig. 2d). STAT3, a transcription factor, is activated by numerous cytokines, growth factors, and proinflammatory cytokines and plays an important role in the cell cycle, tumour, and hepatic inflammation (*33-35*). The effect of NDEA on oxidative damage and proinflammatory and immunological responses in ICR mice was found, which was to enhance the levels of TNF-α and IL-6, thereby accelerating phosphorylation of STAT3 (*36*). Activated STAT3

exclusively interacts with or collaborates with nuclear EGFR at the COX-2 promoter region, causing enhanced COX-2 expression, which is linked to inflammatory responses and cancer (*37*). A previous study reported that TLR4 activation may regulate the COX-2/PGE2/STAT3 loop in hepatocellular carcinoma (HCC) cells (*38*). LSP156, along with the findings from western blotting, reduces COX-2 protein levels by blocking STAT3 activation and TLR4 expression to help protect the liver and prevent damage.

Effect of LSP156 on gut microbiota in NDEA-induced mice

The liver, being the organ most affected by the gut microbiota, is increasingly considered a crucial and prospective therapeutic target for several complex disorders, especially HCC (*39*). Numerous investigations have demonstrated that polyphenols serve as alternative agents for modulating the gut microbiota (*40*). We investigated the impact of LPS156 on the gut microbiota by assessing the intestinal microbial population structure using gene sequencing. Fig. 3a shows Venn diagrams that compare the variety of gut microbes in the two more effective treatment groups (AH and BH), the control group (C), and the model group (M).

The total number of OTUs in the model group increased when compared with the control group, whereas more specific OUTs existed. Furthermore, the OTUs of the treatment groups (AH and BH) were more coincidental with group C than with group M. Based on the relative abundance of intestinal flora among different groups depicted in Fig. 3b and Fig. 3c, the species composition of groups M and C exhibited alterations; furthermore, *Bacteroidales* and *Clostridiales* emerged as the predominant orders, with the abundance of *Bacteroidales* and *Lactobacillales* in the model group significantly surpassing that of group C. The abundances of *Bacteroidales*, *Lactobacillales*, and *Enterobacteriales* in the group M were higher than those in the group C. In contrast to group C, *Clostridiales*, *Campylobacterales*, *Erysipelotrichales*, and *Deferribacterales* exhibited reduced abundance. LPS156 treatment significantly decreased *Bacteroidales* (AH: 3.2 %, BH: 4.2 %) and *Lactobacillales* (AH: 10.2 %, BH: 1.9 %) populations (Fig. 3b). Notably, LPS156 restored these diminished orders to control levels, demonstrating its regulatory effect on gut microbiota homeostasis. Taxonomic analysis revealed differential abundance of seven families (*Lachnospiraceae, Bacteroidaceae, Lactobacillaceae, Ruminococcaceae, Prevotellaceae, Helicobacteraceae,* and *Porphyromonadaceae*) compared to controls. NDEA intervention specifically reduced key families, including *Lachnospiraceae* (11.7 %), *Helicobacteraceae* (5.9 %), and *Rikenellaceae* (2.5 %) at the family level (Fig. 3c). The LEfSe analysis identified taxonomic distinctions: Lactobacillus and Arthromitus dominated group M, whereas *Marvinbryantia* characterised group C. The AH group displayed greater microbial diversity

than BH, predominantly comprising *Bifidobacteriaceae*, *Actinobacteria*, and *Turicibacter* (Fig. 3d). Polyphenol reportedly enhanced *Lachnospiraceae*, *Clostridiales*, *Campylobacterales*, *Erysipelotrichales*, and *Deferribacteriales*—taxa associated with the mitigation of gastrointestinal and hepatic inflammation, including fibrotic progression (*41*). Concordantly, elevated Bacteroidetes abundance observed in murine models (aligning with our data) may constitute a risk factor for endogenous infections or colorectal carcinogenesis (*42*).

Metabolic pathway of the gut microbiota

Functional genomic profiling using the Kyoto Encyclopaedia of Genes and Genomes (KEGG) pathway analysis revealed significant N-nitroso diethylamine (NDEA)-induced perturbations in microbial metabolic pathways, particularly carbohydrate metabolism, terpenoid-quinone biosynthesis, and proteolytic processing (Fig. 4). Comparative analysis demonstrated LSP156's superior therapeutic efficacy over prophylactic effects in mitigating NDEA-driven hepatotoxicity, with pathway restoration correlating to injury attenuation.

Associations between the phenotype and gut microbial community

Correlation analysis of the top 30 gut microbiota with host parameters revealed significant associations between microbial taxa and oxidative/hepatic/inflammatory markers (Fig. 5). Oxidative stress markers showed that *Ruminiclostridium*, *Roseburia*, *Oscillibacter*, Mucispirillum, *Lachnospiraceae*_NK4A136_group, *Helicobacter*, and *Alistipes* were positively correlated with SOD/GSH levels, whereas lactate dehydrogenase (LDH) exhibited inverse associations. Hepatic function indices demonstrated positive correlations with *Ruminococcaceae* and *Escherichia shigella*, contrasting with *Anaeroplasma*'s negative associations with ALT, AST, AKP, and TBiL ($p<0.05$). Notably, *Lachnoclostridium* displayed anti-inflammatory properties through negative correlations with TNF-α and IL-6. *Bacteroides* and *Lactobacillus* maintained positive correlations with pro-inflammatory hepatic indicators (LDH, AKP, TBiL, TNF-α, and IL-6) despite overall microbiota divergence. Pathophysiological correlation mapping further revealed *Bacteroidetes*' significant association with TNF-α/IL-6 ($p<0.05$), suggesting this phylum mediates inflammatory cascades in NDEA-induced hepatotoxicity through both direct and indirect pathways. Lactobacillaceae demonstrated positive correlations with hepatic injury biomarkers (AKP, ALT and TBiL) and pro-inflammatory cytokines, suggesting immune-mediated pathways potentiate its beneficial microbial expansion. LSP156 supplementation attenuated NDEA-induced hepatotoxicity by restoring microbial homeostasis, highlighting gut–liver axis modulation as its protective mechanism (*43*).

CONCLUSIONS

Polyphenolic compounds mitigate hepatopathology by attenuating oxidative stress, modulating anti-inflammatory signalling, and altering the gut–liver axis. Our results demonstrate that LSP156 increases body weight and organ indices, reduces oxidative damage and inflammatory responses, alleviates liver tissue injury, and regulates the STAT3/COX-2 signalling pathway in NDEA-induced liver injury mice. Furthermore, LSP156 alleviates gut microbiota dysbiosis and adjusts microbial composition to reduce liver damage. This study highlights the connection between STAT3/COX-2 signalling and gut microbiota alterations, providing a comprehensive therapeutic approach that could significantly influence the management of liver diseases.

ACKNOWLEDGEMENT

Thanks to Dr. Bo Wei and Tianru Zhang for the help with the revision and improvement of the paper.

FUNDING

This work was financially supported by the National Natural Science Foundation of China (31270060), Domestic visiting programs for outstanding young talents in universities (JY0002221-2022), Microbial experimental technique (JY000188-tzpy032). Funding for this work was provided by the Major Natural Science Research Project of colleges and universities of Anhui Province (Grant Nos. 2024AH040182 and KJ2021zd0164), and modern agricultural industry practice centers on integrated production and instruction (2023cj2x011).

CONFLICT OF INTEREST

The authors declare no conflict of interest.

AUTHORS' CONTRIBUTIONS

T.T. Chen contributed to obtaining methodology, investigation, software, data curation, and writing-Original draft. D. Liu contributed to designing/performing experiments, processing/interpreting data, funding acquisition, writing-review and editing. M. Ye contributed to conceptualization, project administration, supervision, funding acquisition, writing-reviewing and editing.

ORCID ID

D. Liu https://orcid.org/0000-0001-5846-3196

M.Ye https://orcid.org/0000-0002-0730-3528

REFERENCES

1. Park JE, Seo JE, Lee JY, Kwon H. Distribution of seven N-nitrosamines in food. Toxicol Res. 2015;31:279-88.
https://doi.org/10.5487/TR.2015.31.3.279

2. Farré MJ, Insa S, Lamb A, Cojocariu C, Gernjak W. Occurrence of N-nitrosamines and their precursors in Spanish drinking water treatment plants and distribution systems. Environ Sci Water Res Technol. 2020;6(1):210-20.
https://doi.org/10.1039/c9ew00912d

3. Lim DS, Roh TH, Kim MK, Kwon YC, Choi SM, Kwack SJ, *et al*. Risk assessment of N-nitrosodiethylamine (NDEA) and N-nitrosodiethanolamine (NDELA) in cosmetics. J Toxicol Env Heal A. 2018;81:465-80.
https://doi.org/10.1080/15287394.2018.1460782

4. Pinprayoon O, Mae W. Migration of N-nitrosamines from rubber gloves for handling food - Effect of extraction media. IOP Conf Series: Mater Sci Eng. 2019;548:012022.
https://doi.org/10.1088/1757-899X/548/1/012022

5. Sallan S, Kaban G, Oğraş ŞŞ, Çelik M, Kaya M. Nitrosamine formation in a semi-dry fermented sausage: Effects of nitrite, ascorbate and starter culture and role of cooking. Meat Sci. 2020;159:107917.
https://doi.org/10.1016/j.meatsci.2019.107917

6. Elguindy NM, Yacout GA, El Azab EF. Amelioration of DENA-induced oxidative stress in rat kidney and brain by the essential oil of *Elettaria cardamomum*. Beni-Suef U J Basic. 2018;7(3):299-305.
https://doi.org/10.1016/j.bjbas.2018.02.005

7. El-Ashmawy NE, El-Bahrawy HA, Shamloula MM, El-Feky OA. Biochemical/metabolic changes associated with hepatocellular carcinoma development in mice. Tumor Biol. 2014;35:5459-66.
https://doi.org/10.1007/s13277-014-1714-6

8. Perumal S, Langeshwaran K, Selvaraj J, Ponnulakshmi R, Shyamaladevi B, Balasubramanian MP. Effect of diosmin on apoptotic signaling molecules in N-nitrosodiethylamine-induced hepatocellular carcinoma in experimental rats. Mol Cell Biochem. 2018;449:27-37.
https://doi.org/10.1007/s11010-018-3339-3

9. Tripathy A, Thakurela S, Sahu MK, Uthansingh K, Singh A, Narayan J, Kumari R. Fatty changes associated with N-Nitrosodiethylamine (DEN) induced hepatocellular carcinoma: a role of sonic hedgehog signaling pathway. Gene Cancer. 2020;11:66-82.
https://doi.org/10.18632/genesandcancer.203

10. Ostry V, Malir F, Toman J, Grosse Y. Mycotoxins as human carcinogens-the IARC Monographs classification. Mycotoxin Res. 2017;33:65-73.
https://doi.org/10.1007/s12550-016-0265-7
11. Yamada KI, Yamamiya I, Utsumi H. In *vivo* detection of free radicals induced by diethylnitrosamine in rat liver tissue. Free Radic Bio Med. 2006;40(11):2040-6.
https://doi.org/10.1016/j.freeradbiomed.2006.01.031
12. Fan T, Sun G, Zhao L, Cui X, Zhong R. Metabolic activation and carcinogenesis of tobacco-specific nitrosamine N'-nitrosonornicotine (NNN): A density function theory and molecular docking study. Int J Environ Res Public Health. 2019;16(2):178-98.
https://doi.org/10.3390/ijerph16020178
13. Rothschild D, Weissbrod O, Barkan E, Kurilshikov A, Korem T, Zeevi D, *et al*. Environment dominates over host genetics in shaping human gut microbiota. Nature. 2018;555(7695):210-5.
https://doi.org/10.1038/nature25973
14. Rowland I, Gibson G, Heinken A, Scott K, Swann J, Thiele I, *et al*. Gut microbiota functions: metabolism of nutrients and other food components. Eur J Nutr. 2018;57:1-24.
https://doi.org/10.1007/s00394-017-1445-8
15. Tripathi A, Debelius J, Brenner DA, Karin M, Loomba R, Schnabl B, *et al*. The gut–liver axis and the intersection with the microbiome. Nat Rev Gastro Hepat. 2018;15(7):397-411.
https://doi.org/10.1038/s41575-018-0011-z
16. Gong S, Lan T, Zeng L, Luo H, Yang X, Li NA, *et al*. Gut microbiota mediates diurnal variation of acetaminophen induced acute liver injury in mice. J Hepatol. 2018;69(1):51-9.
https://doi.org/10.1016/j.jhep.2018.02.024
17. Seki E, Schnabl B. Role of innate immunity and the microbiota in liver fibrosis: crosstalk between the liver and gut. J Physiol. 2012;590(3):447-58.
https://doi.org/10.1113/jphysiol.2011.219691
18. Acharya C, Bajaj JS. Altered microbiome in patients with cirrhosis and complications. Clin Gastroenterol H. 2019;17(2):307-21.
https://doi.org/10.1016/j.cgh.2018.08.008
19. Shavandi A, El-Din Ahmed Bekhit A, Saeedi P, Izadifar Z, Bekhit AA, *et al*. Polyphenol uses in biomaterials engineering. Biomaterials. 2018;167:91-6.
https://doi.org/10.1016/j.biomaterials.2018.03.018
20. Zong S, Ji J, Li J, Yang QH, Ye M. Physicochemical properties and anticoagulant activity of polyphenols derived from *Lachnum singerianum*. J Food Drug Anal. 2017;25(4):837-44.
https://doi.org/10.1016/j.jfda.2016.08.011

21. Schneider CA, Rasband WS, Eliceiri KW. NIH Image to ImageJ: 25 years of image analysis. Nat Methods. 2012;9:671–5.
https://doi.org/10.1038/nmeth.2089
22. Bolger AM, Lohse M, Usadel, B. Trimmomatic: A flexible trimmer for Illumina sequence data. Bioinformatics. 2014;30:2114–20.
https://doi.org/10.1093/bioinformatics/btu170
23. Caporaso JG, Kuczynski J, Stombaugh J, Bittinger K, Bushman FD. QIIME allows analysis of high-throughput community sequencing data. Nature Meth. 2010;7:335–6.
https://doi.org/10.1038/nmeth.f.303
24. Rognes T, Flouri T, Nichols B, Quince C, Mahé F. VSEARCH: a versatile open source tool for metagenomics. PeerJ. 2016; 4: e2584.
https://doi.org/10.7717/peerj.2584
25. GraphPad Prism, v. 8.0, GraphPad Inc, San Diego, California, USA; 2020. Available from: https://www.graphpad.com/guides/prism/8/statistics/
26. Kasdallah-Grissa A, Mornagui B, Aouani E, Hammami M, El May M, Gharbi N, *et al*. Resveratrol, a red wine polyphenol, attenuates ethanol-induced oxidative stress in rat liver. Life Sci. 2007;80(11):1033-39.
https://doi.org/10.1016/j.lfs.2006.11.044
27. Goldberg DM, Watts C. Serum enzyme changes as evidence of liver reaction to oral alcohol. Gastroenterology. 1965;49:256-61.
https://doi.org/10.1093/forestry/38.2.247
28. Liu B, Zhang J, Sun P, Yi R, Han X, Zhao X. Raw bowl tea (Tuocha) polyphenol prevention of nonalcoholic fatty liver disease by regulating intestinal function in mice. Biomolecules. 2019;9(9):435-55.
https://doi.org/10.3390/biom9090435
29. Bartsch H, Hietanen E, Malaveille C. Carcinogenic nitrosamines: free radical aspects of their action. Free Radic Bio Med. 1989;7(6):637-44.
https://doi.org/10.1016/0891-5849(89)90144-5
30. Yang F, Shang L, Wang S, Liu Y, Ren H, Zhu W, *et al*. TNFα-mediated necroptosis aggravates ischemia-reperfusion injury in the fatty liver by regulating the inflammatory response. Oxid. Med. Cell. Longev. 2019;(1):1-14.
https://doi.org/10.1155/2019/2301903

31. Chaudhari N, Talwar P, Parimisetty A, Lefebvre d'Hellencourt C, Ravanan P. A molecular web: endoplasmic reticulum stress, inflammation, and oxidative stress. Front Cell Neurosci. 2014;8:213-28.
https://doi.org/10.3389/fncel.2014.00213

32. Valko M, Leibfritz D, Moncol J, Cronin MT, Mazur M, Telser J. Free radicals and antioxidants in normal physiological functions and human disease. Int J Biochem Cell B. 2007;39(1):44-84.
https://doi.org/10.1016/j.biocel.2006.07.001

33. Miller AM, Wang H, Park O, Horiguchi N, Lafdil F, Mukhopadhyay P, *et al*. Anti-inflammatory and anti-apoptotic roles of endothelial cell STAT3 in alcoholic liver injury. Alcoho Clin Exp Res. 2010;34(4):719-25.
https://doi.org/10.1111/j.1530-0277.2009.01141.x

34. Wang H, Lafdil F, Wang L, Park O, Yin S, Niu J, *et al*. Hepatoprotective versus oncogenic functions of STAT3 in liver tumorigenesis. Am J Pathol. 2011;179(2):714-24.
https://doi.org/10.1016/j.ajpath.2011.05.005

35. Bharadwaj U, Kasembeli MM, Robinson P, Tweardy D J. Targeting janus kinases and signal transducer and activator of transcription 3 to treat inflammation, fibrosis, and cancer: rationale, progress, and caution. Pharmacol Rev. 2020;72(2):486-526.
https://doi.org/10.1124/pr.119.018440

36. Agrawal S, Gollapudi S, Su H, Gupta S. Leptin activates human B cells to secrete TNF-α, IL-6, and IL-10 via JAK2/STAT3 and p38MAPK/ERK1/2 signaling pathway. J Clin Immunol. 2011;31:472-8.
https://doi.org/10.1007/s10875-010-9507-1

37. Greenhough A, Smartt HJ, Moore AE, Roberts HR, Williams AC, Paraskeva C, *et al*. The COX-2/PGE 2 pathway: key roles in the hallmarks of cancer and adaptation to the tumour microenvironment. Carcinogenesis. 2009;30(3):377-86.
https://doi.org/10.1093/carcin/bgp014

38. Kim EJ, Raval AP, Perez-Pinzon MA. Preconditioning mediated by sublethal oxygen-glucose deprivation-induced cyclooxygenase-2 expression via the signal transducers and activators of transcription 3 phosphorylation. J Cerebr Blood F Met. 2008;28(7):1329-40.
https://doi.org/10.1038/jcbfm.2008.26

39. Woodhouse CA, Patel VC, Singanayagam A, Shawcross DL. The gut microbiome as a therapeutic target in the pathogenesis and treatment of chronic liver disease. Aliment Pharm Ther. 2018;47(2):192-202.
https://doi.org/10.1111/apt.14397

40. Li Q, Liu F, Liu J, Liao S, Zou Y. Mulberry leaf polyphenols and fiber induce synergistic antiobesity and display a modulation effect on gut microbiota and metabolites. Nutrients. 2019;11(5):1017-32. https://doi.org/10.3390/nu11051017

41. Li L, Tu Y, Dai X, Xiao S, Tang Z, Wu Y, *et al*. The effect of *Abrus cantoniensis* Hance on liver damage in mice. Ecotox Environ Safe. 2023; 66:115560. https://doi.org/10.1016/j.ecoenv.2023.115560

42. Chung L, Orberg ET, Geis AL, Chan JL, Fu K, Shields CED, *et al*. Bacteroides fragilis toxin coordinates a pro-carcinogenic inflammatory cascade via targeting of colonic epithelial cells. NCell Host Microbe. 2018;23(2):203-14. https://doi.org/10.1016/j.chom.2018.02.004

43. Sabino J, Vieira-Silva S, Machiels K, Joossens M, Falony G, Ballet V, *et al*. Primary sclerosing cholangitis is characterised by intestinal dysbiosis independent from IBD. Gut. 2016;65(10):1681-9. https://doi.org/10.1136/gutjnl-2015-311004

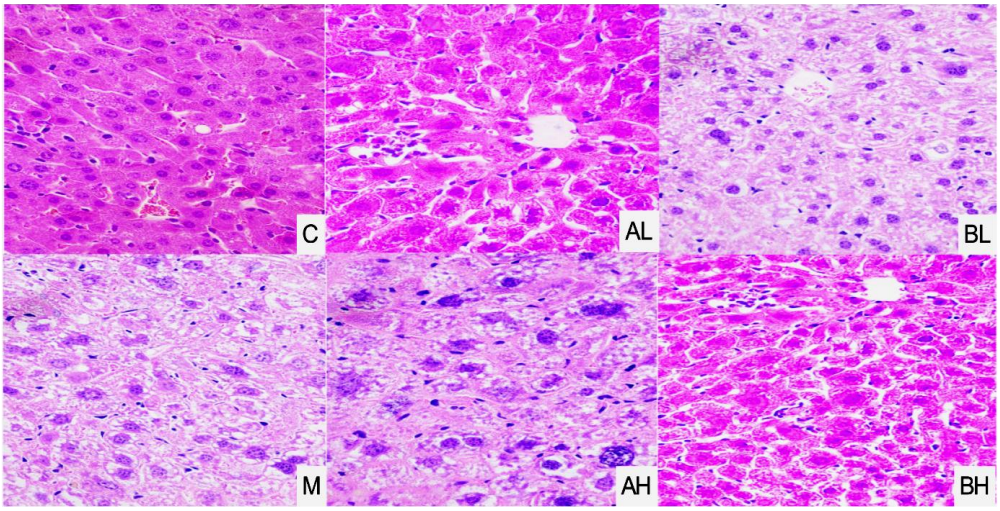

Fig. 1. The statues of hepatic steatosis, hepatocyte morphology and inflammatory cell infiltration were checked by H&E staining (400×)

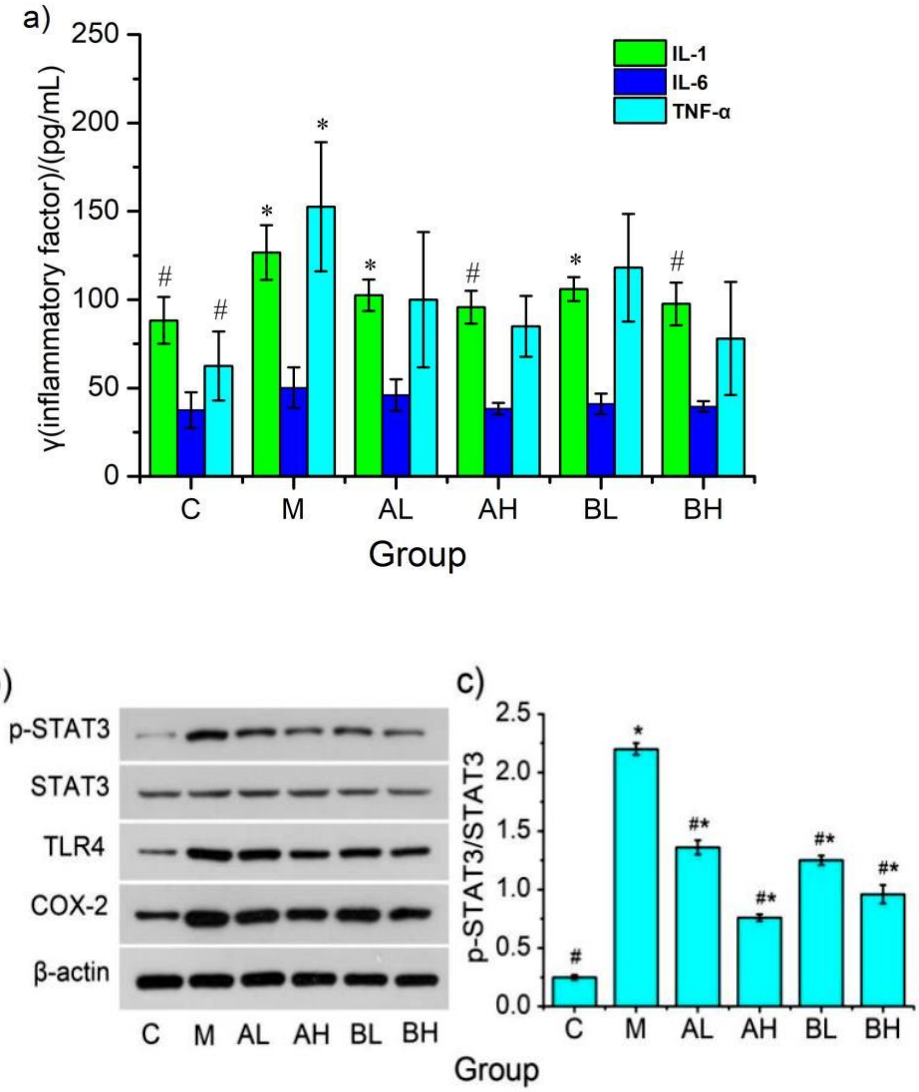

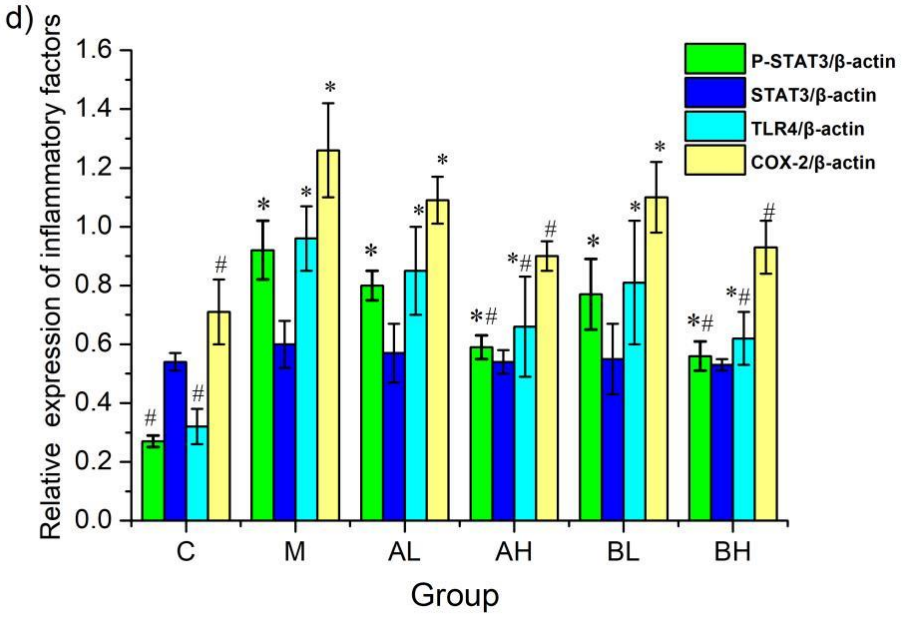

Fig. 2. Effect of LPS156 on inflammatory factors and the critical proteins of STAT3/COX-2 signal pathway in NDEA-induced hepatic injury mice: (a) inflammatory markers IL-6 and TNF-α levels in serum were measured. Data are presented as mean values±S.D., *N*=8. *p<0.05 compared with the control group, and $^{\#}$p<0.05 compared with the model group, (b) protein expression of p-STAT3, STAT3, TLR4 and COX-2 in liver tissues, (c) protein abundance of p-STAT3/STAT3 in liver tissues, showing the degree of activation of STAT3, (d) inflammatory factors proteins expression to β-actin in liver tissue. Data are presented as mean values±S.D., *N*=3. *p<0.05 compared with the control group, and $^{\#}$p<0.05 compared with the model group

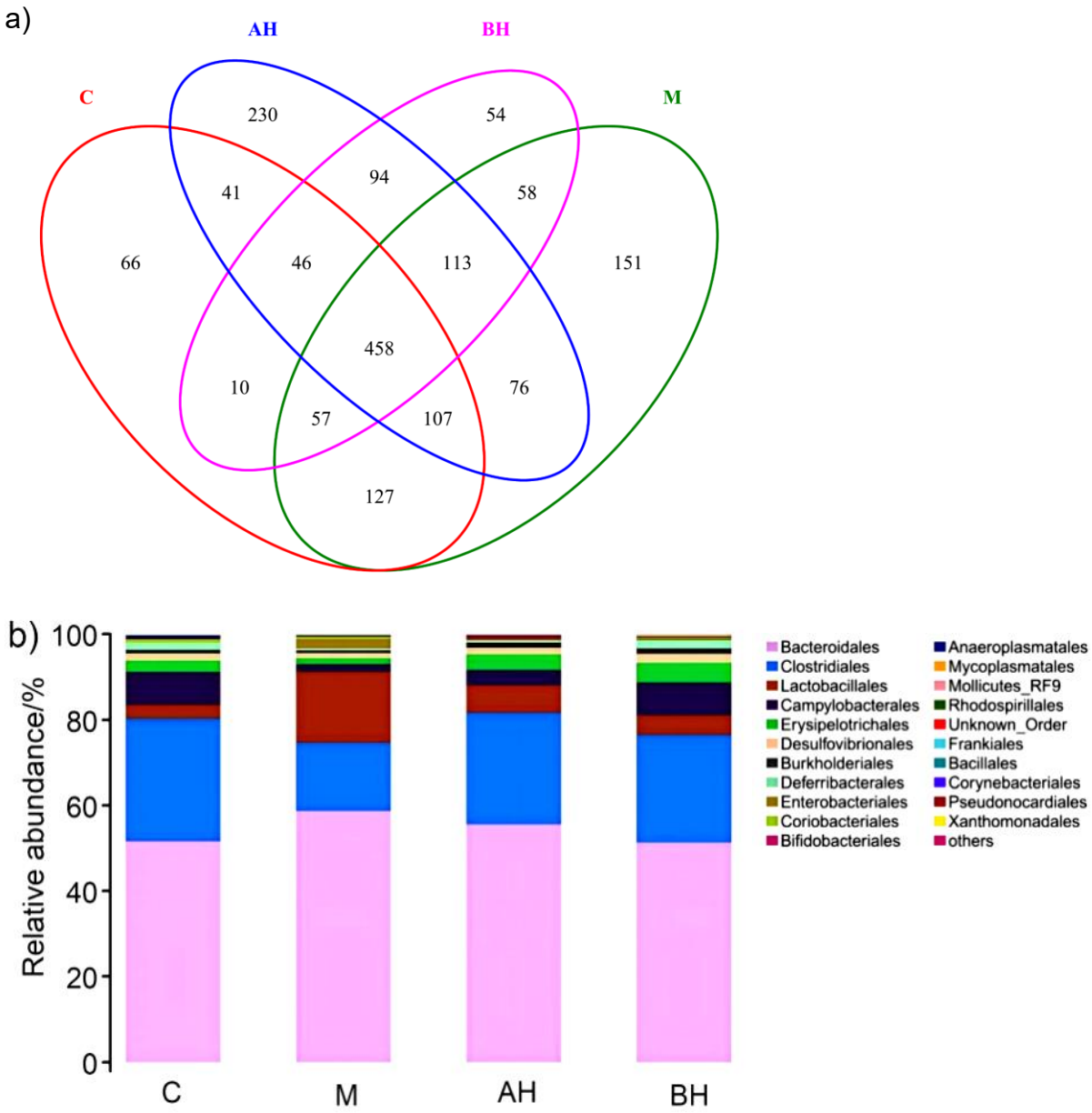

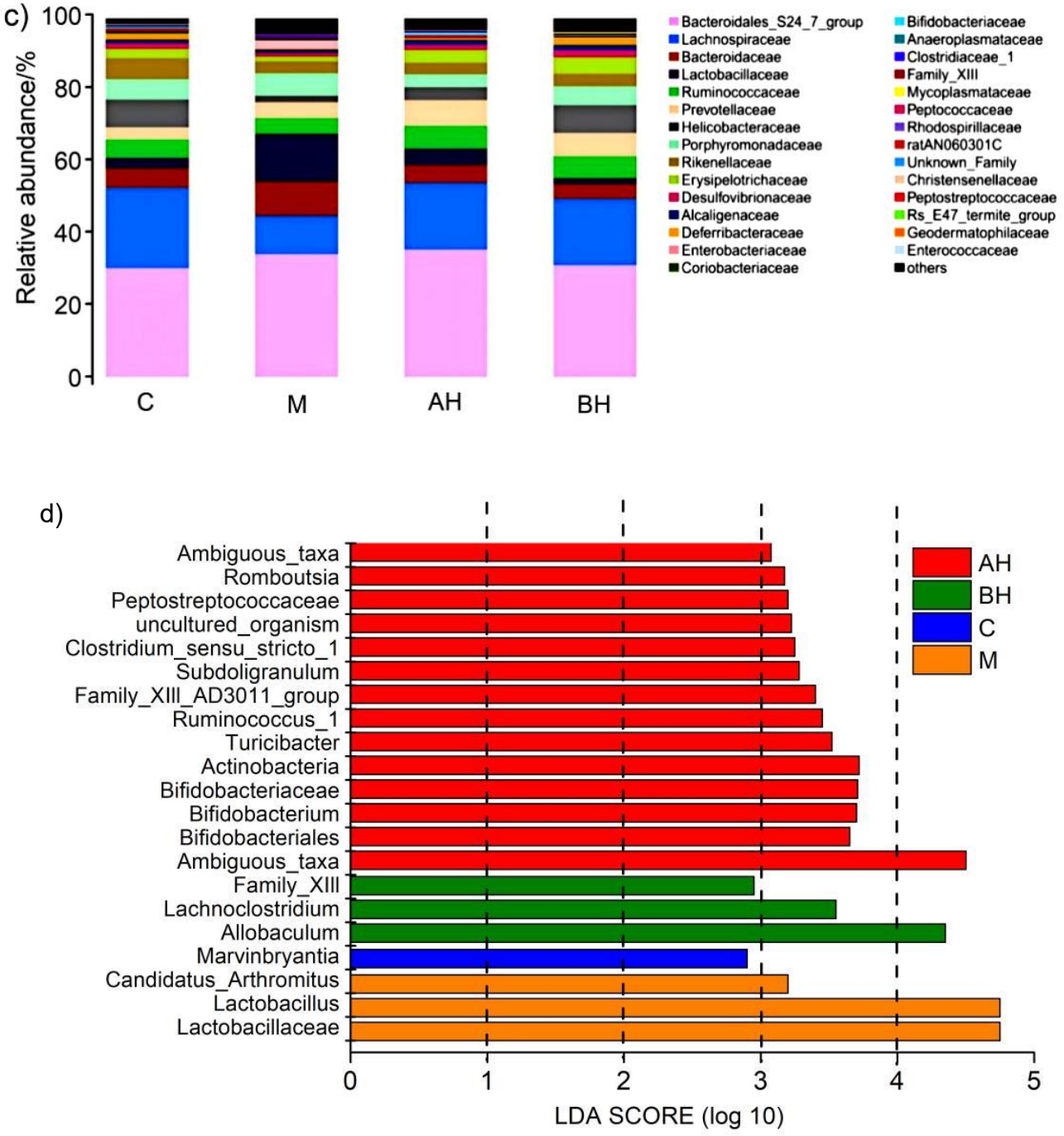

Fig. 3. LPS156 changed the types and variety of gut bacteria in mice with liver damage caused by NDEA: (a) Venn diagrams showing the unique and shared OTUs in the gut microbiota of the respective groups. The presented values are the mean±S.D., *N*=5, (b) a heat map indicating the relative abundance distributions of each group at the order, and (c) family levels of the top 30 (mean value±S.D., *N*=5), (d) LEfSe analysis showing the relative abundance among the different groups in mice

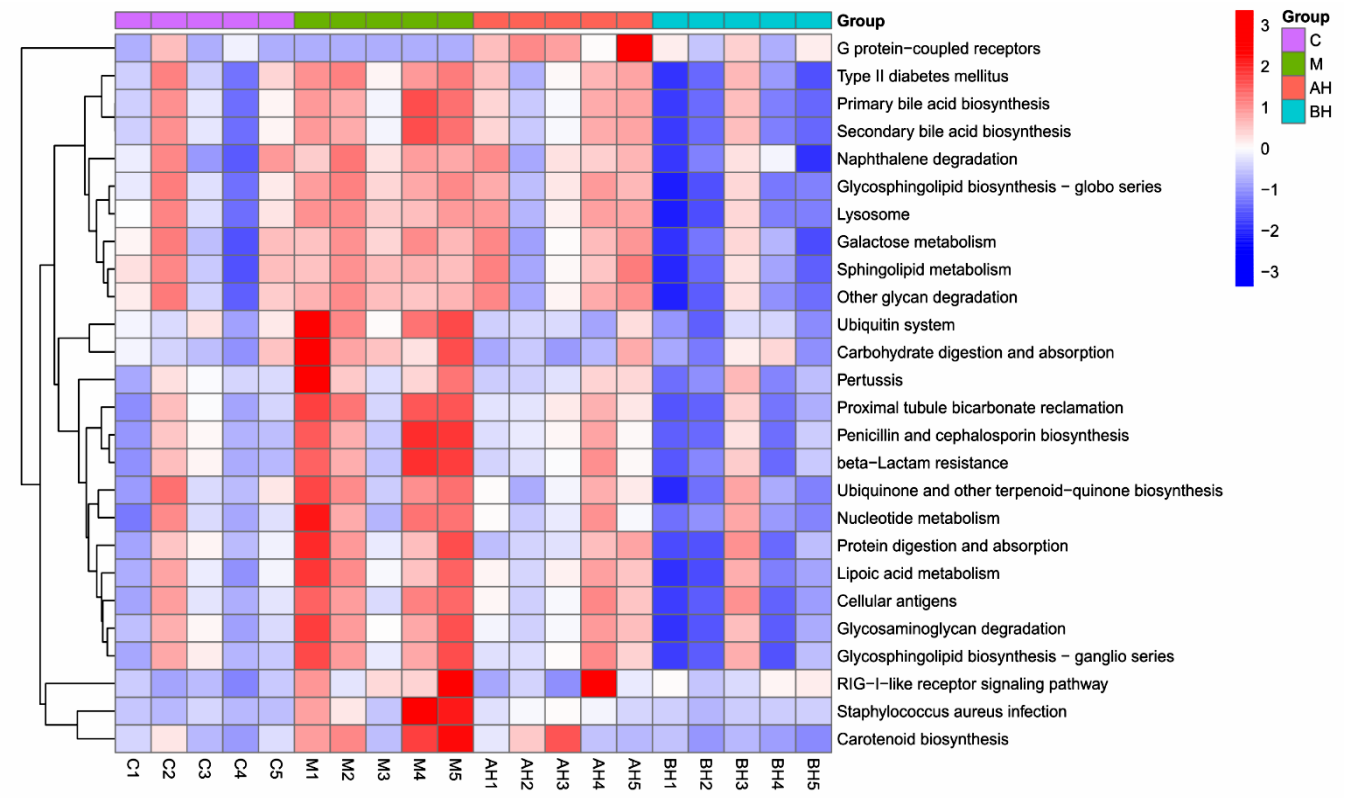

Fig. 4. The predicted difference in the KEGG metabolic pathways of the gut microbiota from different groups

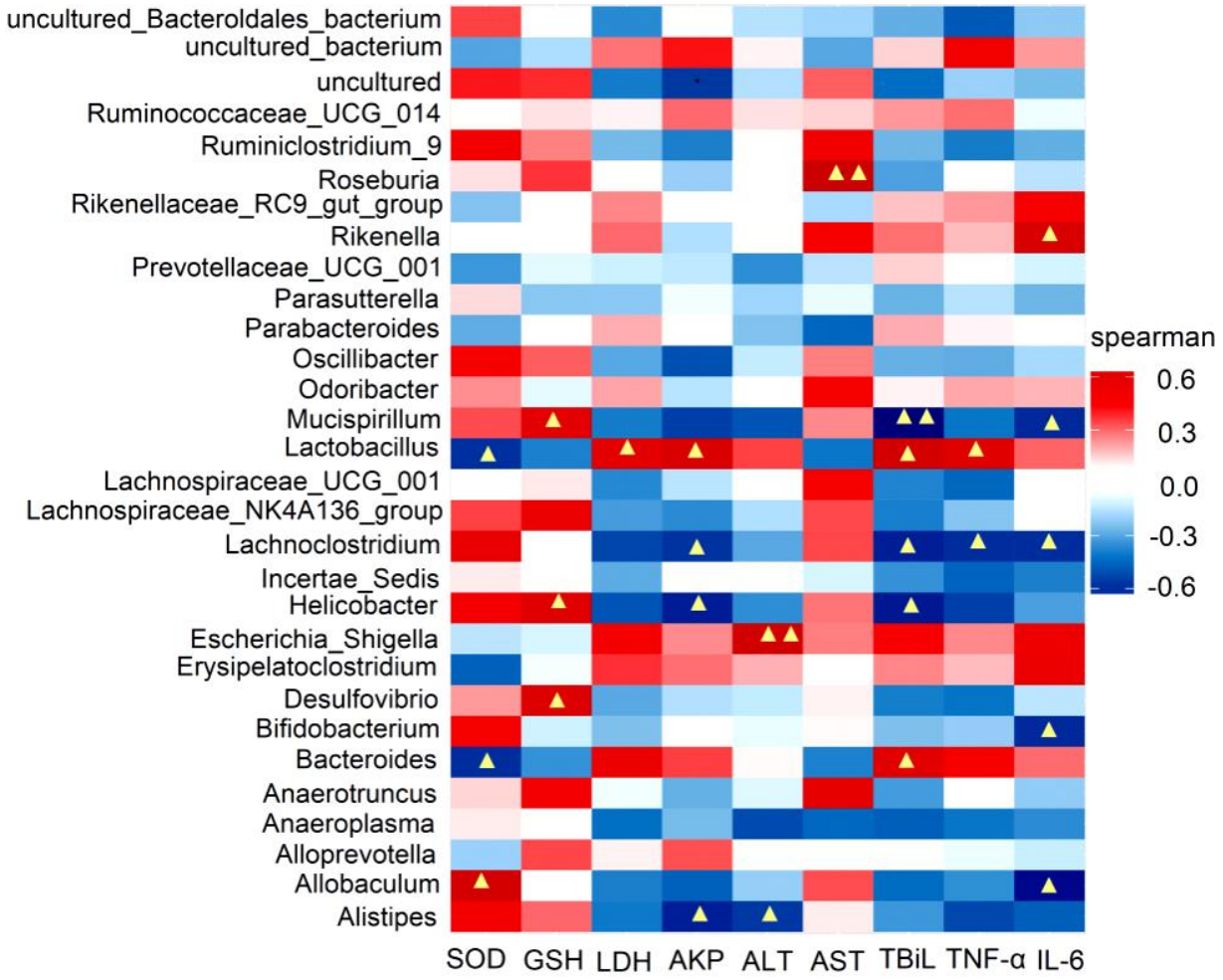

Fig. 5. Heatmap of the correlations between metagenomic genera and phenotype. (▲) indicates a significant correlation ($p<0.05$); (▲▲) indicates a significant correlation ($p<0.01$). The correlation was determined by the Spearman index

Table 1. Effects of LPS156 on the values of ALT, AST, AKP and TBiL

Parameter	C	M	AL	AH	BL	BH
AST activity/(U/g)	6.3±1.2^{b}	13.6±3.7^{a}	10.0±2.7	7.5±1.1^{b}	12.4±2.6	9.6±1.1
ALT activity/(U/g)	18.2±1.9^{b}	30.7±2.6^{a}	28.8±1.8^{a}	26.8±3.2^{a}	27.6±1.3^{a}	22.2±2.8^{b}
AKP activity/(U/g)	103.3±12.1^{b}	580.5±10.9^{a}	395.9±9.6^{ab}	257.3±10.2^{ab}	415.3±11.2^{ab}	196.6±5.2^{ab}
γ(TBil)/(μmol/L)	1.1±0.1^{b}	7.5±0.7^{a}	6.6±0.4^{a}	3.8±0.5^{b}	3.9±0.6^{b}	2.9±0.6^{b}

Data are presented as mean value±S.D., N=8. $^{a}p<0.05$ compared with the control group, and $^{b}p<0.05$ compared with the model group

Table 2. Effects of LPS156 on purtenance indices and oxidative stress parameters

Parameter	C	M	AL	AH	BL	BH
Weight gain/g	12.1±1.2	5.3±2.4^{a}	6.5±1.9^{a}	7.7±2.7^{ab}	6.0±1.3^{a}	7.3±2.1^{ab}
Liver index/(mg/g)	6.0±0.5	5.8±0.7	5.3±0.8	4.9±0.7^{a}	4.5±1.4^{ab}	4.9±1.0^{a}
Kidney index/(mg/g)	1.5±0.2	1.27±0.2	1.4±0.3	1.3±0.1	1.3±0.1	1.3±0.2
Spleen index/(mg/g)	0.3±0.1	0.4±0.1	0.5±0.1	0.4±0.1	0.3±0.1	0.3±0.1
SOD/(U/mg)	1038.2±14.9	860.4±7.4^{a}	956.8±15.5^{b}	997.9±14.1^{b}	1082.8±14.7^{b}	1123.0±28.5^{b}
CAT/(U/mg)	37.6±2.6	27.4±1.8^{a}	29.3±2.1^{a}	29.5±3.8^{a}	28.1±2.7^{a}	30.0±3.9
MDA/(nmol/mg)	3.2±0.5	6.2±0.8^{a}	4.5±0.4^{ab}	3.3±0.3^{b}	4.7±0.2^{ab}	2.7±0.1^{b}
GSH/(μmol/g)	6.5±1.4	4.5±1.2^{a}	5.0±1.1^{a}	5.5±1.2^{b}	4.4±1.0^{a}	5.8±0.6^{b}

Data are presented as mean value±S.D., N=8. $^{a}p<0.05$ compared with the control group, and $^{b}p<0.05$ compared with the model group